HHS Public Access

Author manuscript

Biomaterials. Author manuscript; available in PMC 2018 April 01.

Published in final edited form as:

Biomaterials. 2017 April ; 123: 107–117. doi:10.1016/j.biomaterials.2017.01.038.

Engineering of a hybrid nanoparticle-based nicotine nanovaccine as a next-generation immunotherapeutic strategy against nicotine addiction: a focus on hapten density

Zongmin Zhao[†], **Kristen Powers**[‡], **Yun Hu**[†], **Michael Raleigh**[§], **Paul Pentel**[§], and **Chenming Zhang**[†,*]

[†]Department of Biological Systems Engineering, Virginia Tech, Blacksburg, VA 24061, United States

[‡]Department of Biological Science, Virginia Tech, Blacksburg, VA 24061, United States

[§]Minneapolis Medical Research Foundation, Minneapolis, MN 55404, United States

Abstract

Although vaccination is a promising way to combat nicotine addiction, most traditional hapten-protein conjugate nicotine vaccines only show limited efficacy due to their poor recognition and uptake by immune cells. This study aimed to develop a hybrid nanoparticle-based nicotine vaccine with improved efficacy. The focus was to study the impact of hapten density on the immunological efficacy of the proposed hybrid nanovaccine. It was shown that the nanovaccine nanoparticles were taken up by the dendritic cells more efficiently than the conjugate vaccine, regardless of the hapten density on the nanoparticles. At a similar hapten density, the nanovaccine induced a significantly stronger immune response against nicotine than the conjugate vaccine in mice. Moreover, the high- and medium-density nanovaccines resulted in significantly higher anti-nicotine antibody titers than their low-density counterpart. Specifically, the high-density nanovaccine exhibited better immunogenic efficacy, resulting in higher anti-nicotine antibody titers and lower anti-carrier protein antibody titers than the medium- and low-density versions. The high-density nanovaccine also had the best ability to retain nicotine in serum and to block nicotine from entering the brain. These results suggest that the hybrid nanoparticle-based nicotine vaccine can elicit strong immunogenicity by modulating the hapten density, thereby providing a promising next-generation immunotherapeutic strategy against nicotine addiction.

Graphical abstract

[*]Corresponding author. Address: 210 Seitz Hall, Department of Biological Systems Engineering, Virginia Tech, Blacksburg, VA 24061, Voice: +1-(540)231-7601. Fax: +1-(540)231-3199. chzhang2@vt.edu.

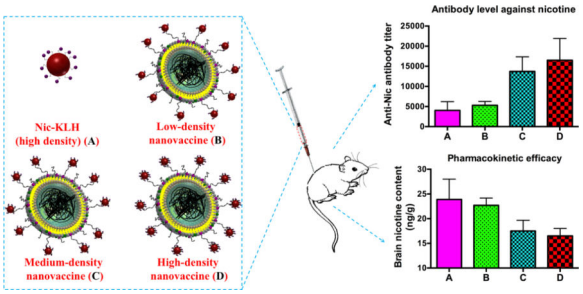

Keywords

Nicotine addiction; nicotine vaccine; hybrid nanoparticle; antibody; hapten density

1. Introduction

Tobacco smoking remains to be the leading cause of preventable diseases and premature deaths. It is responsible for nearly 6 million deaths and significant economic losses each year worldwide.[1, 2] Despite the use of pharmacological treatments, such as nicotine replacement therapy and nicotine agonists/antagonists, only a small percentage of treated smokers (10–25%) are able to successfully quit smoking.[3–5] Therefore, more efficient approaches are needed to combat tobacco addiction.

Nicotine vaccines induce the production of antibodies that specifically bind to nicotine in serum, thereby blocking its entrance into the brain; they have been presented as an attractive strategy to treat nicotine addiction.[6, 7] Over the past several decades, many nicotine vaccines have been found to achieve high immunogenicity and pharmacokinetic efficacy in preclinical trials.[8–11] However, to date, all human clinical trials of conjugate nicotine vaccines have not achieved the expected efficacies.[12] The phase 2 clinical studies of NicVax and NicQβ revealed that while the overall smoking cessation rate was not enhanced in the study group in comparison to the placebo group, the quit rate improved in the top 30% of the study group subjects that had the highest antibody titers.[13, 14] Together with our previously reported physiologically-based-pharmacokinetic-modeling data,[15] these clinical findings suggest that while the basic concept of using immunotherapy to promote smoking cessation is solid, future vaccines have to be able to elicit high titers of antibodies to be effective.

A variety of approaches to strengthen the immunogenicity of traditional conjugate nicotine vaccines have been investigated, including the design of hapten structure,[16, 17] the modulation of the linker position and composition,[8] the selection of carrier proteins,[10] the use of different adjuvants,[18] the application of multivalent vaccines,[19–22] and the optimization of administration routes[23]. However, as the immune system is relatively poor at recognizing small soluble protein antigens [24, 25], traditional conjugate nicotine vaccines bear a serious innate shortcoming, poor recognition and internalization by immune cells. Even with the help of alum adjuvants to form particulate antigens, conjugate nicotine vaccines cannot be easily tuned to have optimal physicochemical properties (shape, size, and charge) for uptake. Furthermore, conjugate nicotine vaccines suffer from several other innate

shortfalls, such as fast degradation, difficulty integrating with molecular adjuvants, and short immune persistence, which limit their immunogenic outcomes.[26]

Nanoparticles (NPs) have been widely used for the efficient delivery of drugs, proteins, and vaccines.[27–33] Based on the hypothesis that NPs might provide a new strategy to overcome the limitations of conjugate nicotine vaccines, this study aimed to develop a lipid-poly(lactic-co-glycolic acid) (lipid-PLGA) hybrid nanoparticle (NP)-based nicotine vaccine to improve the immunogenicity of the conjugate nicotine vaccine. This hybrid NP-based nicotine nanovaccine was designed to enhance the delivery and presentation of B cell epitopes and T cell help proteins, both of which are required to induce an effective humoral immune response, to immune cells. Because hapten density might play an important role in the ability of immune cells to recognize nanovaccine particles, we investigated its influence on the immunogenicity of the nicotine nanovaccines. Various nanovaccine NPs with different hapten densities were fabricated, and their physicochemical properties and epitope density were characterized. The *in vitro* uptake of the hapten-protein conjugate and nanovaccine particles was studied in immature dendritic cells (DCs). The immunogenicity and pharmacokinetic efficacy of three nanovaccines (low-, medium-, and high-hapten density) were tested in mice. Finally, histopathological analysis was used to determine the safety of the proposed hybrid NP-based nanovaccine.

2. Materials and methods

2.1 Materials

Lactel® 50:50 PLGA (acid-terminated) was purchased from Durect Corporation (Cupertino, CA, USA). 2,4,6-trinitrobenzenesulfonic acid (TNBSA), Alexa Fluor 350 (AF350), Alexa Fluor 647 (AF647), and keyhole limpet hemocyanin (KLH) were purchased from Thermo Fisher Scientific Inc. (Rockford, IL, USA). 1,2-Dioleoyl-3-trimethylammonium-propane (DOTAP), cholesterol (CHOL), 1,2-distearoyl-sn-glycero-3-phosphoethanolamine-N-[maleimide(polyethylene glycol)-2000] (ammonium salt) (DSPE-PEG2000-maleimide), and 1,2-diphytanoyl-sn-glycero-3-phosphoethanolamine-N-(7-nitro-2-1,3-benzoxadiazol-4-yl) (ammonium salt) (NBD-PE) were purchased from Avanti Polar Lipids Inc. (Alabaster, AL, USA). O-succinyl-3’-hydroxymethyl-(±)-nicotine (Nic) hapten was purchased from Toronto Research Chemicals (North York, ON, Canada). All other chemicals were of analytical grade.

2.2 Preparation of lipid-PLGA NPs

PLGA NPs were prepared using a double emulsion solvent evaporation method. In brief, 50 mg of PLGA was dissolved in 2 mL of dichloromethane (oil phase). Two hundred μL of ultrapure water was added to the oil phase. The mixture was emulsified by sonication for 10 min using a Branson M2800H Ultrasonic Bath sonicator (Danbury, CT, USA). The resultant primary emulsion was added dropwise to 12 mL of 0.5% w/v poly(vinyl alcohol) solution. The suspension was emulsified by sonication using a sonic dismembrator (Model 500; Fisher Scientific, Pittsburg, PA, USA) at an amplitude of 70% for 40 s. The resultant secondary emulsion was stirred overnight to allow complete dichloromethane evaporation.

PLGA NPs were collected by centrifugation at 10,000 *g*, 4 °C for 30 min (Beckman Coulter Avanti J-251, Brea, CA, USA). Pellets were washed three times using ultrapure water.

Lipid-PLGA NPs were assembled using a film-hydration-sonication method as described previously.[34] In brief, 15 mg of lipid mixture dissolved in chloroform consisting of DOTAP, DSPE-PEG2000-maleimide, and CHOL (90:5:5 in moles) was evaporated to form a lipid film. One mL of 0.01 M pH 7.4 phosphate buffer saline (PBS) was added to hydrate the lipid film. The resultant suspension was sonication for 5 min in a Branson M2800H Ultrasonic Bath sonicator. Fifteen mg of PLGA NPs suspended in DI water (10 mg/ml) was added and mixed with the above liposome suspension. Subsequently, the mixture was sonicated in an ice-water bath using a bath sonicator for 5 min. Lipid-PLGA NPs were collected by centrifugation at 10,000 *g*, 4 °C for 30 min.

2.3 Assembly of nicotine vaccine NPs with different hapten density

Nic-KLH conjugates were synthesized using a carbodiimide-mediated reaction. In brief, Nic-hapten of various equivalents of KLH was mixed with appropriate amounts of 1-ethyl-3-(3-dimethylaminopropyl)carbodiimide hydrochloride (EDC) and Sulfo-N-hydroxysulfosuccinimide (NHS) in activation buffer (0.1 M MES, 0.5 M NaCl, pH 6.0) and incubated at room temperature for 15 min. The mixture was added to 5 mg of KLH, which was dissolved in coupling buffer (0.1 M sodium phosphate, 0.15 M NaCl, pH 7.2). After the overnight reaction, unconjugated Nic-hapten and byproducts were eliminated by dialyzing against 0.01 M PBS (pH 7.4) at room temperature for 24 h. The number of Nic-haptens on Nic-KLH was determined by measuring the difference in the number of remaining lysine groups on the surface of KLH before and after hapten conjugation using a TNBSA based method. In brief, KLH and Nic-KLH conjugates were prepared at a concentration of 1 mg/mL. Two hundred μL of the protein solution was taken and mixed with 200 μL of 4% $NaHCO_3$ solution. Two hundred μL of 0.1% TNBSA solution was added to the mixture and incubated at 37 °C for 1 h, and the absorbance was read at 335 nm. Hapten density of KLH was calculated from the differences between the O.D. of the control and the conjugates.

Nanovaccine NPs were assembled by attaching Nic-KLH conjugates onto the surface of lipid-PLGA hybrid NPs via a thiol-maleimide-mediated method. In brief, an appropriate amount of Traut's reagent was added to the Nic-KLH conjugate (containing 3 mg of KLH), which was dissolved in 0.1 M pH 8.0 bicarbonate buffer and incubated for 1 h. Nic-KLH was attached to lipid-PLGA NPs by reacting to the thiolated Nic-KLH with the appropriate amount of lipid-PLGA NPs in 0.1 M pH 8.0 bicarbonate buffer for 2 h. NPs were collected by centrifugation at 10,000 *g*, 4 °C for 30 min. Unattached Nic-KLH in the supernatant was quantified by the BCA assay. The lipid layer of hybrid NPs was labeled by NBD-PE, and the number of lipid-PLGA NPs was counted by flow cytometry. Hapten density (number of haptens per NP) was approximated by the following formula, $D_{nic}=(AF_{Nic\text{-}KLH}*M_{Nic\text{-}KLH}*D_{Nic\text{-}KLH}*N_A)/N_{NPs}$, where D_{nic}, $AF_{Nic\text{-}KLH}$, $M_{Nic\text{-}KLH}$, $D_{Nic\text{-}KLH}$, N_A, and N_{NPs} represent hapten density per NP, Nic-KLH association efficiency, moles of KLH associated on 1 mg of NPs, hapten density of Nic-KLH, Avogadro constant, and NP number per 1 mg of NPs, respectively. Vaccine NPs were lyophilized and stored at 2 °C for later use.

2.4 Characterization of NPs

The successful assembly of nanovaccine NPs was validated using confocal laser scanning microscopy (CLSM). Fluorescent vaccine NPs—in which the lipid layer, PLGA layer, and KLH were labeled by NBD, Nile red, and AF350, respectively—were prepared according to a similar method as described above with minor modifications. In brief, PLGA NPs containing Nile red were fabricated by a double emulsion solvent evaporation method, wherein the appropriate amount of Nile red was dissolved in the oil phase. The lipid layer was labelled by adding 5% w/w of NBD-PE into the lipid mixture. AF350 was conjugated to KLH through an EDC-mediated reaction. NPs were imaged by a Zeiss LSM 510 Laser Scanning Microscope (Carl Zeiss, Germany). The morphology of NPs was studied using transmission electron microscopy (TEM). In brief, NP suspensions (2 mg/mL) were dropped onto a 300-mesh Formvar-coated copper grid. The remaining suspension was removed with wipes after standing for 10 min. The samples were negatively stained for 20 s using freshly-prepared 1% phosphotungstic acid. The samples were then washed twice using ultrapure water. The dried samples were imaged on a JEOL JEM 1400 transmission electron microscope (JEOL Ltd., Tokyo, Japan). The physicochemical properties of NPs, including particle size and zeta potential, were measured by the Dynamic Light Scattering method and Laser Doppler Micro-electrophoresis method on a Malvern Nano ZS Zetasizer (Malvern Instruments Ltd, Worcestershire, United Kingdom), respectively.

2.5 Cellular uptake of vaccine particles by DCs

The uptake of vaccine particles by DCs was quantitatively measured by flow cytometry. JAWSII (ATCC® CRL-11904™) immature DCs were cultured in alpha minimum essential medium (80% v/v) supplemented with ribonucleosides, deoxyribonucleosides, 4 mM L-glutamine, 1 mM sodium pyruvate, 5 ng/mL murine GM-CSF, and fetal bovine serum (20% v/v) at 37 °C, 5% CO_2. Cells were seeded into 24-well plates (2×10^6/well) and cultured overnight. In order to compare the cellular uptake of conjugate vaccine and nanovaccine, AF647, a model of Nic-hapten, was used instead of Nic-hapten to prepare vaccine particles to provide fluorescence. Cells were treated with vaccine particles containing the same amount of KLH (10 μg). To compare the cellular uptake of nanovaccine particles with different hapten densities, 5% (w/w) NBD-PE was added to the lipid layer of nanoparticles to provide fluorescence. Cells were treated with nanovaccine particles containing the same amount of hybrid NPs (50 μg). After incubation for 2 h, the medium was immediately removed, and the cells were washed three times with 0.01 M pH 7.4 PBS. Cells were detached from the culture plates using Trypsin/EDTA solution and centrifuged at 200 *g* for 10 min. Cell pellets were re-suspended in 0.01 M pH 7.4 PBS. Samples were immediately analyzed on a flow cytometer (BD FACSAria I, BD, Franklin Lakes, NJ, USA).

The uptake and intracellular distribution of vaccine particles were qualitatively determined by CLSM. Cells were seeded into a 2-well chamber slide (2×10^5/chamber), and cultured overnight. The original medium was replaced with 2 mL of fresh medium containing vaccine particles. After incubation for 2 h, the medium was discarded, and the cells were washed three times using 0.01 M pH 7.4 PBS. One mL of freshly-prepared 4% (w/v) paraformaldehyde was added to each well to fix the cells for 15 min. The fixed cells were washed three times with PBS and were made permeable by adding 0.5 mL of 0.1% (v/v)

Triton™ X-100 for 15 min. After washing the cells three times using PBS, the nuclei of cells were stained with DAPI. The intracellular distribution of NPs was visualized on a Zeiss LSM 510 Laser Scanning Microscope.

2.6 Immunization of mice with nicotine vaccines

All animal studies were carried out following the National Institutes of Health (NIH) guidelines for animal care and use. Animal protocols were approved by the Institutional Animal Care and Use Committee at Virginia Polytechnic Institute and State University. Female Balb/c mice (6–7 weeks of age, 16–20 g, 8 per group) were immunized subcutaneously on Days 0, 14, and 28 with vaccines of negative control (KLH associated lipid-PLGA NPs), Nic-KLH with alum, low-density nanovaccine, low-density nanovaccine with alum, medium-density nanovaccine, medium-density nanovaccine with alum, high-density nanovaccine, and high-density nanovaccine with alum. For vaccine groups without alum adjuvant, the mice were injected with vaccine particles (containing 25 μg of protein antigen) that were suspended in 200 μL of 0.01 M pH 7.4 PBS. In the vaccine with alum adjuvant groups, the mice were injected with vaccine particles (containing 25 μg of protein antigen) that were suspended in 100 μL of PBS and mixed with 100 μL of alum (10 mg/mL), and the mixture was used to immunize mice. The alum (aluminum hydroxide, Alhydrogel® adjuvant 2%) was purchased from Invivogen (San Diego, CA, USA). Blood samples were collected on Days 0, 12, 26, 40, and 54.

2.7 Measurement of nicotine-specific IgG antibody (NicAb) titer and anti-carrier protein antibody titer

The NicAb titers in serum were determined by ELISA as described previously.[35] Anti-KLH antibody titers were measured using a similar ELISA protocol, and KLH was used as the coating material. Antibody titer was defined as the dilution factor at which absorbance at 450 nm declined to half maximal.

2.8 Pharmacokinetic study in mice

Female Balb/c mice (6–7 weeks of age, 16–20 g, 4–5 per group) were immunized with the same protocol as described in the previous context. On Day 54, mice were administrated with 0.03 mg/Kg nicotine subcutaneously. Mice were euthanized under anesthesia 4 min after nicotine challenge, and the blood and brain were collected. Nicotine contents in serum and brain tissues were analyzed by GC/MS according to a method reported previously. [20]

2.9 Preliminary evaluation of the safety of nanovaccines

The safety of the nicotine nanovaccines was preliminarily evaluated in mice by monitoring the body weight change and histopathological analysis. To investigate the body weight change during the study, mice were weighed before primary immunization and once a week after that. Histopathological analysis of tissues from immunized mice was performed to examine the lesions caused by the administration of nanovaccine NPs. In brief, different mouse organs were fixed with 10% formalin, followed by cutting the organs according to a standard protocol. Tissue blocks were then embedded in paraffin, and the routine sections

were stained with hematoxylin and eosin. The stained sections were imaged on a Nikon Eclipse E600 light microscope, and pictures were captured using a Nikon DS-Fi1 camera.

2.10 Statistical analysis

Comparisons between two groups were performed by unpaired student's t-test. Comparisons among multiple groups were conducted by one-way ANOVA followed by Tukey's HSD analysis. Differences were considered significant if p-values were less than 0.05.

3. Results and discussion

As shown in Scheme 1, the NP-based nicotine nanovaccine in this study was formed by conjugating multiple Nic-KLH conjugates to the surface of one hybrid NP. The PLGA core not only serves as a scaffold to support the lipid layer and stabilize the nanovaccine system, but also endows the nanovaccine with the property of small particles to achieve improved recognition and internalization by immune cells. The lipid layer was composed of DOTAP, CHOL, and DSPE-PEG2000-maleimide. The DSPE-PEG2000-maleimide component enables the association of hapten-carrier protein conjugates (Nic-KLH) onto the surface of lipid-PLGA NPs. Nic hapten that is a B cell epitope is conjugated to the carrier protein (KLH) to be immunogenic. The KLH carrier protein provides sufficient T cell help peptides to promote the activation and maturation of B cells. The Nic hapten density of the nicotine nanovaccine was modulated to achieve an optimal immunological efficacy.

3.1 Validation of the conjugate chemistry and characterization of the structure of nanovaccine NPs

The nanovaccine NPs assembled in this study are designed to have a structure composed of a PLGA core, a lipid shell, and multiple Nic-KLH conjugates. Confocal laser scanning microscopy (CLSM) was used to characterize the nanovaccine structure and verify the conjugate chemistry of hapten. The PLGA, lipid, and KLH layers were labeled with Nile Red, NBD, and AF350 fluorescence, respectively. As shown in Fig. 1, almost all particles were co-labeled with the three fluorescent colors, indicating that lipids were successfully coated around PLGA NPs to form a hybrid core-shell structure, and KLH was associated to the surface of NPs with very high efficiency. Meanwhile, AF350 was a model of Nic-hapten, having similar size and the same reactive group (NHS ester). In this study, Nic-hapten was attached to KLH by the EDC/NHS-mediated conjugate chemistry, in which the carboxylic groups of Nic were activated by EDC/NHS to form semi-stable Nic-NHS esters that could readily react with the amino groups of KLH. AF350 was conjugated to KLH efficiently, validating the feasibility of the hapten conjugate chemistry.

The structure of the nanovaccine NPs was further investigated using TEM. Fig. 2A shows the TEM images exhibiting the morphology of PLGA NPs, liposomes, lipid-PLGA hybrid NPs, and nanovaccine NPs. All four NPs were of spherical shapes. A distinguishing core-shell structure, which was shown as a bright PLGA core and a dark lipid shell, was observed on lipid-PLGA NPs (Fig. 2A (c)), indicating the successful coating of lipids onto PLGA NPs. As shown in Fig. 2A (d), multiple black dots, which were Nic-KLH conjugates, were located on the surface of hybrid NPs, confirming the efficient association of Nic-KLH. KLH

is a large carrier protein that is composed of KLH1 and KLH2 subunits, both of which are around 400 kDa.[36] The large size makes it visible in the TEM images. The average size of NPs increased from 90.8 nm to 107.0 nm upon lipid coating and further increased to 121.3 nm after Nic-KLH associating (Fig. 2B). Bare PLGA NPs had a negative zeta-potential (−14.3 mV) (Fig. 2C), which may be attributed to the carboxylic acid terminal groups of the PLGA polymer used in this study. Upon lipid coating and Nic-KLH conjugation, the zeta potential of NPs changed to 12.6 mV for Lipid-PLGA NPs as the liposome is positively charged (Fig. 2C), and then to 4.16 mV for nanovaccine NPs (Fig. 2C) because Nic-KLH is negatively charged (−17.3 ± 2.3 mV).

3.2 Preparation and characterization of nanovaccines with different hapten density

Various molar excess of Nic-hapten to KLH was applied for the conjugating reaction of hapten on KLH. The hapten density of the prepared nanovaccines is shown in Fig. 3A. The increased hapten density from NKLP-A to NKLP-I verified the feasibility of modulating the Nic hapten density by changing the molar ratios of hapten to KLH in the preparation process. To date, most reported hapten-protein conjugate nicotine vaccines have hapten density ranging from 2 to 100 per protein molecule,[10, 37, 38] depending on the available lysine groups and conjugate chemistry. Noticeably, the design of the hybrid-NP based nicotine nanovaccine significantly increased the epitope numbers per particle over conventional conjugate nicotine vaccines, potentially contributing to an enhanced epitope recognition by B cells. Each NKLP-C, NKLP-F, and NKLP-I nanovaccine NP carried approximately 29×10^3, 146×10^3, and 319×10^3 Nic haptens, respectively (Table 1). Statistical analysis revealed that the hapten densities of NKLP-C, NKLP-F, and NKLP-I are significantly different ($p<0.001$). Thus, in this study, NKLP-C, NKLP-F, and NKLP-I were selected as low-, medium-, and high-density nanovaccines for *in vivo* immunogenicity study. The physicochemical properties of different hapten density nanovaccines were characterized and shown in Fig. 3B and Table 1. The average zeta potentials of NKLP-C, NKLP-F, and NKLP-I nanovaccine NPs were 4.16 mV, 3.92 mV, and 3.86 mV, respectively. The positively charged surface of nanovaccine NPs will enhance their interaction with the negatively charged surface of immune cells,[39] thereby promoting cellular uptake of the nanovaccines. The average size of NKLP-C, NKLP-F, and NKLP-I was 121.3 nm, 123.8 nm, and 121.2 nm, respectively. According to Fig. 3C, all three nanovaccine NPs exhibited narrow size distributions, with most of the NPs less than 200 nm, which were in agreement with the small PDI (0.21–0.24, Table 1) and uniform size in the TEM images (Fig. 2A(d)). It has been reported that size is a critical parameter influencing the efficacy of nanoparticle vaccines. Particles of 20–200 nm will efficiently enter the lymphatic system, while by contrast, particles that are larger than 200–500 nm do not efficiently enter lymph capillaries in a free form.[40–42] The size of the nanovaccines in this study was relatively optimal and will hopefully result in high immunogenicity.

3.3 Cellular uptake of nanovaccine NPs by dendritic cells (DCs)

Efficient capture, internalization, and processing of nicotine containing antigens by DCs largely determine the outcomes of vaccination. Traditional nicotine-protein conjugate vaccines suffer from the shortfall of poor recognition and internalization by immune cells. Here, we compared the uptake of nanovaccine NPs (AF647-KLP) to nicotine-KLH

conjugate vaccine particles (AF647-KLH) by DCs. Nic-hapten was substituted by AF647 to render KLH fluorescent, and the density of AF647 on KLH of either AF647-KLH or AF647-KLP was identical. As shown in Fig. 4B and Fig. 4C, the mean fluorescence intensity (M.F.I.) of AF647 in the AF647-KLP group was over 500% more than that in the AF647-KLH group, suggesting that more protein antigens were taken up by DCs in the nanovaccine NP group within the same time. The uptake and distribution of particles in DCs were also examined by CLSM. As shown in Fig. 4A, in agreement with the flow cytometry results, brighter AF647 fluorescence was observed in the AF647-KLP group compared to the AF647-KLH group, indicating again that DCs took up antigens more efficiently when treated with AF647-KLP. The conjugation of multiple Nic-KLH to one hybrid nanoparticle may increase the availability of antigens for uptake, thus contributing to an enhanced antigen internalization. Meanwhile, the immune system prefers to recognize and take up particulate pathogens (such as bacteria and virus) and is relatively invisible to small soluble protein antigens.[24, 25] The stable and spherical lipid-PLGA hybrid nanoparticles endowed the nanovaccine with the property of small particles. This particulate nature together with the relatively optimal physicochemical properties is beneficial for the improved uptake by DCs. The internalization of more protein antigens by DCs enhanced by the lipid-PLGA NP delivery vehicles will benefit many of the immunogenic outcomes of nicotine nanovaccines. The uptake and processing of protein antigens is a critical prerequisite for T helper cell formation, which is necessary for B cell activation in humoral immunity.[26, 43] Therefore, the more protein antigens internalized by DCs, the more T helper cells may be generated, causing more B cells to be activated, and finally leading to a better immunogenic efficacy of nicotine vaccines.

The uptake of different hapten density nanovaccine NPs by DCs was characterized. As shown in Fig. 4D, for all the nanovaccine groups, including KLP (non-hapten-conjugated nanovaccine), NKLP-C, NKLP-F, and NKLP-I, over 96% of the cells were stained by the NBD fluorescence within 2 h. This demonstrated that all the nanovaccine NPs, regardless of hapten density, were rapidly taken up by dendritic cells. Furthermore, as demonstrated in Fig. 4E, the M.F.I. of NBD of blank cells was less than 250, while by contrast, the values were around 6000 for all four nanovaccine groups and no marked difference was detected in terms of NBD fluorescence intensity. This indicated that DCs could take up all different hapten density nanovaccine NPs efficiently, and hapten density would not influence this process discriminately. This similar uptake efficiency can be attributed to the similar physicochemical properties (size and charge) of nanovaccine NPs despite the difference in hapten densities. The uptake of nanovaccine NPs was further confirmed by CLSM, shown in Fig. 4F, in which the lipid-PLGA NPs and KLH were labeled by NBD and AF647, respectively. Co-localized, bright green and red fluorescence showing simultaneously in all recorded cells verified that the DCs rapidly and efficiently took up the nanovaccine NPs. Despite the similar uptake behavior of different hapten density nanovaccine NPs by DCs, Nic hapten density is expected to impact the recognition and activation of nicotine-specific B cells, and thereby influencing the efficacy of nanovaccines.

3.4 Immunogenicity of different hapten density nicotine nanovaccines

The goal of nicotine vaccines is to induce the production of specific antibodies that bind to nicotine and thereby block its entry into the brain. Previous studies have shown that the pharmacokinetic efficacy of nicotine vaccines closely correlates with the antibody concentration elicited.[11, 44] The phase 2 clinical trials of NicVax revealed that only the top 30% of subjects with the highest antibody titers showed improved smoking cessation rates compared to the placebo.[13] Therefore, the presence of high antibody titers is one of the most critical factors influencing the efficacy of nicotine vaccines.

Fig. 5A shows the time-course results of anti-nicotine antibody titers, demonstrating that administration of all nicotine vaccines resulted in a steady increase of anti-nicotine IgG antibody titers along the study period. Particularly a sharp increase was observed after the first boost injection (on Day 26). In this study, the hapten density on KLH of the Nic-KLH conjugate vaccine and high-density nanovaccine were identical. The antibody titers in the high-density nanovaccine with or without alum groups were much higher (4–10 fold) than that in the Nic-KLH with Alum group in all the studied days. This enhanced immunogenicity was in agreement with the enhanced internalization of antigens caused by the lipid-PLGA hybrid NP delivery system (Fig. 4B). These results were consistent with previous reports. It was reported that a tetrahedral DNA nanostructure delivery system could effectively enhance antigen uptake and induce strong and long-lasting antibody responses against antigens.[45] The ability of different hapten density nanovaccines to induce nicotine-specific antibodies was compared. As shown in Fig. 5A, the high-density nanovaccine induced the highest antibody titers compared to the low- and medium-density nanovaccines along the entire study period. Particularly, at the end of the study (on Day 54), the average antibody titer of the low-density without alum group was 5300, and increased by 7%, 159%, 166%, 211%, and 257% to 5700, 13700, 14100, 16500, and 18900, in groups of low-density with alum, medium-density with and without alum, high-density with and without alum, respectively. As shown in Fig. 5B, statistical analysis revealed that there were significant differences between the high-/medium-density groups and low-density groups, regardless of the presence of alum or not ($p<0.05$). Although no statistically significant differences were observed between the high- and medium-density groups ($p>0.05$), the high-density nanovaccines resulted in more responders of high antibody titers. Specifically, based on a cutoff of antibody titer >15000, the percentage of high-titer responders was 37.5%, 37.5%, 50%, and 75% in medium-density with and without alum groups, high-density with and without alum groups, respectively. The increased immunogenicity of nanovaccines with higher hapten density could be attributed to the evidence that the nanovaccine NPs with more haptens would have more chances to be recognized by naïve B cells, thereby activating more nicotine-specific B cells and strengthening the immune response. These results are not completely consistent with previous studies reporting the influence of hapten density on the efficacy of nicotine-protein conjugate vaccines. Miller et al. reported that nicotine 6-hexanoic acid-KLH conjugate nicotine vaccine generated higher antibody titers with a density of 100 compared to 22.[10] In another study, McCluskie et al. showed that stronger immune responses were obtained with 5-aminoethoxy-nicotine-CRM conjugate vaccines having hapten density of 11–18, with weaker responses above the range and more variable

responses below the range.[37] Pravetoni et al. reported that the antibody titer was highest with a hapten/KLH ratio of 700:1 in a 1-SNic-KLH conjugate vaccine.[22]

The titers of anti-KLH antibody were measured to evaluate the influence of hapten density of nanovaccines on the production of carrier protein specific antibodies. As shown in Fig. 6, the anti-KLH antibody titer of the negative control group, in which no hapten was conjugated, was around 90000. Interestingly, in contrast, the anti-KLH antibody titers were reduced by 30.6%, 24.5%, 55.4%, 51.3%, 71.8%, and 68.6% in groups of low-density, low-density with alum, medium-density, medium-density with alum, high-density, and high-density with alum, respectively. Evidently, the anti-carrier protein antibody titers decreased with the increase of hapten density. Statistical analysis revealed significant differences in the anti-KLH antibody titers of different hapten density nanovaccine groups ($p<0.05$). This is probably because hapten conjugation masks the immunogenic epitopes on the carrier protein surface. A low anti-carrier protein antibody titer is considered beneficial for the vaccine design in this study. First, the utilization of nanovaccine to produce antibodies against carrier protein antibody rather than nicotine is a wastage of nanovaccine particles. The low-level production of anti-carrier protein antibody would leave more nanovaccines available to elicit anti-nicotine antibodies. Second, anti-carrier protein antibodies may neutralize the carrier protein on the surface of nanovaccine particles that are injected during the booster immunizations. Therefore, a low anti-carrier protein antibody level might minimally impair the immunological efficacy of nicotine nanovaccines.

3.5 Pharmacokinetic efficacy of different hapten density nicotine nanovaccines

Ultimately, nicotine vaccines are designed to retain nicotine in serum and block it from entering the brain. As shown in Fig. 7A, the serum nicotine level was 5.75 ng/mL for the low-density nanovaccine group and increased by 160% and 204% to 15.0 ng/mL and 17.5 ng/mL for the medium- and high-density nanovaccine groups, respectively. This suggests the medium- and high-density nanovaccines had better efficacy in retaining nicotine in serum than the low-density nanovaccine, and particularly, the high-density nanovaccine exhibited the best efficacy. Fig. 7B shows the results of brain nicotine levels in mice vaccinated with different hapten density nanovaccines. The brain nicotine levels of Nic-KLH with alum group, low-density group, medium-density group, and high-density group, were reduced by 14.0%, 17.2%, 36.7%, and 40.0% compared to that of the negative control group. Statistical analysis revealed that the brain nicotine level for the high-density nanovaccine group was significantly lower than that of the Nic-KLH with alum group, suggesting that the use of lipid-PLGA hybrid NPs as delivery vehicles considerably enhanced the pharmacokinetic efficacy of the conjugate nicotine vaccine. In addition, the medium- and high-density nanovaccines resulted in considerably higher brain nicotine reduction than the low-density nanovaccine, and statistical analysis showed that the high-density nanovaccine had a significantly lower brain nicotine level than the low-density nanovaccine. This indicated that the high-density nanovaccine exhibited the best efficacy in blocking nicotine from entering the brain. The pharmacokinetic data were in concordance with the results of anti-nicotine antibody titers. Both the results of anti-nicotine antibody titers and pharmacokinetic efficacy revealed that the immunological efficacy of the hybrid NP-based nicotine nanovaccine could be enhanced by modulating the hapten density.

3.6 Preliminary safety of nicotine nanovaccines

Mouse organs, including heart, kidney, liver, lung, and spleen, were examined by histopathological analysis after administration of nicotine vaccines. Fig. 8A shows the representative histopathological images of the negative control group and nicotine vaccine groups. As for the three different hapten density nanovaccines, mouse organs exhibited similar characteristics. The histopathological review revealed no significant lesions in the five organs of mice of each treatment and control groups. Mouse body weight was monitored as an indicator of vaccine safety along the study period. As shown in Fig. 8B, no body weight losses were detected for all the groups, indicating that the administration of nicotine vaccines did not impose apparent adverse impacts on mouse growth. Meanwhile, no short-term effects, including local site reaction, apparent abnormal behavior, and elevation in temperature, were found among mice treated with the nicotine vaccine formulations. The above preliminary safety results prove that the lipid-PLGA NP based nicotine nanovaccines, regardless of hapten density, are of distinguishing safety.

4. Conclusion

In this study, lipid-polymeric NP-based nicotine nanovaccines with different hapten density were synthesized and characterized *in vitro* and *in vivo*. The *in vitro* results suggested that all nanovaccine NPs, regardless of hapten density, were taken up by dendritic cells efficiently. Moreover, nanovaccine NPs were internalized by dendritic cells more efficiently compared to the hapten-KLH conjugate particles in terms of internalized antigens. The *in vivo* immunization study in mice indicated that the nanovaccine resulted in a 570% higher antibody titer than the Nic-KLH conjugate vaccine at a similar hapten density. Furthermore, the medium- and high-density nanovaccines exhibited significantly higher immunogenicity compared to the low-density nanovaccine. In addition, although no significant differences in antibody titers were detected between the high- and medium-density nanovaccines, the high-density nanovaccine resulted in more responders of high antibody titers (>15000). The pharmacokinetic study in mice suggested that the high hapten density nanovaccine had the best efficacy in blocking nicotine from entering the brain. The histopathological study showed that none of the different hapten density nanovaccines caused any apparent toxic effects to mouse organs. All these findings suggest that the immunogenicity of the lipid-polymeric NP based nicotine nanovaccines can be enhanced by modulating hapten density, and therefore providing a promising next-generation immunotherapeutic strategy to treating nicotine addiction.

Acknowledgments

This work was financially supported by National Institute on Drug Abuse (U01DA036850). We thank Ms. Kathy Lowe for her assistance on TEM imaging of NPs. We thank Dr. Tanya LeRoith for providing help on histopathological analysis.

References

1. Benowitz NL. Nicotine addiction. New Engl. J. Med. 2010; 362:2295–2303. [PubMed: 20554984]

2. Lockner JW, Lively JM, Collins KC, Vendruscolo JCM, Azar MR, Janda KD. A conjugate vaccine using enantiopure hapten imparts superior nicotine-binding capacity. J. Med. Chem. 2015; 58:1005–1011. [PubMed: 25493909]

3. McCarthy DE, Piasecki TM, Lawrence DL, Jorenby DE, Shiffman S, Fiore MC, Baker TB. A randomized controlled clinical trial of bupropion SR and individual smoking cessation counseling. Nicotine Tob. Res. 2008; 10:717–729. [PubMed: 18418793]

4. Stapleton JA, Watson L, Spirling LI, Smith R, Milbrandt A, Ratcliffe M, Sutherland G. Varenicline in the routine treatment of tobacco dependence: a pre-post comparison with nicotine replacement therapy and an evaluation in those with mental illness. Addiction. 2008; 103:146–154. [PubMed: 18028247]

5. Carpenter MJ, Jardin BF, Burris JL, Mathew AR, Schnoll RA, Rigotti NA, Cummings KM. Clinical strategies to enhance the efficacy of nicotine replacement therapy for smoking cessation: a review of the literature. Drugs. 2013; 73:407–426. [PubMed: 23572407]

6. Raupach T, Hoogsteder PH, Onno van Schayck CP. Nicotine vaccines to assist with smoking cessation: current status of research. Drugs. 2012; 72:e1–e16.

7. Shen XY, Orson FM, Kosten TR. Vaccines against drug abuse. Clin. Pharmacol. Ther. 2012; 91:60–70. [PubMed: 22130115]

8. Pryde DC, Jones LH, Gervais DP, Stead DR, Blakemore DC, Selby MD, Brown AD, Coe JW, Badland M, Beal DM, Glen R, Wharton Y, Miller GJ, White P, Zhang NL, Benoit M, Robertson K, Merson JR, Davis HL, McCluskie MJ. Selection of a novel anti-nicotine vaccine: influence of antigen design on antibody function in mice. Plos One. 2013; 8

9. Hieda Y, Keyler DE, VandeVoort JT, Kane JK, Ross CA, Raphael DE, Niedbalas RS, Pentel PR. Active immunization alters the plasma nicotine concentration in rats. J. Pharmacol. Exp. Ther. 1997; 283:1076–1081. [PubMed: 9399979]

10. Miller KD, Roque R, Clegg CH. Novel anti-nicotine vaccine using a trimeric coiled-coil hapten carrier. Plos One. 2014; 9

11. Pravetoni M, Keyler DE, Raleigh MD, Harris AC, LeSage MG, Mattson CK, Pettersson S, Pentel PR. Vaccination against nicotine alters the distribution of nicotine delivered via cigarette smoke inhalation to rats. Biochem. Pharmacol. 2011; 81:1164–1170. [PubMed: 21333633]

12. De Biasi M, McLaughlin I, Perez EE, Crooks PA, Dwoskin LP, Bardo MT, Pentel PR, Hatsukami D. Scientific overview: 2013 BBC plenary symposium on tobacco addiction. Drug Alcohol. Depen. 2014; 141:107–117.

13. Hatsukami DK, Jorenby DE, Gonzales D, Rigotti NA, Glover ED, Oncken CA, Tashkin DP, Reus VI, Akhavain RC, Fahim REF, Kessler PD, Niknian M, Kalnik MW, Rennard SI. Immunogenicity and smoking-cessation outcomes for a novel nicotine immunotherapeutic. Clin. Pharmacol. Ther. 2011; 89:392–399. [PubMed: 21270788]

14. Cornuz J, Zwahlen S, Jungi WF, Osterwalder J, Klingler K, van Melle G, Bangala Y, Guessous I, Muller P, Willers J, Maurer P, Bachmann MF, Cerny T. A Vaccine against nicotine for smoking cessation: a randomized controlled trial. Plos One. 2008; 3

15. Saylor K, Zhang CM. A simple physiologically based pharmacokinetic model evaluating the effect of anti-nicotine antibodies on nicotine disposition in the brains of rats and humans. Toxicol. Appl. Pharm. 2016; 307:150–164.

16. Meijler MM, Matsushita M, Altobelli LJ, Wirsching P, Janda KD. A new strategy for improved nicotine vaccines using conformationally constrained haptens. J. Am. Chem. Soc. 2003; 125:7164–7165. [PubMed: 12797775]

17. de Villiers SHL, Lindblom N, Kalayanov G, Gordon S, Baraznenok I, Malmerfelt A, Marcus MM, Johansson AM, Svensson TH. Nicotine hapten structure, antibody selectivity and effect relationships: Results from a nicotine vaccine screening procedure. Vaccine. 2010; 28:2161–2168. [PubMed: 20060511]

18. Lockner JW, Ho SO, McCague KC, Chiang SM, Do TQ, Fujii G, Janda KD. Enhancing nicotine vaccine immunogenicity with liposomes. Bioorg. Med. Chem. Lett. 2013; 23:975–978. [PubMed: 23313243]

19. Cornish KE, de Villiers SHL, Pravetoni M, Pentel PR. Immunogenicity of individual vaccine components in a bivalent nicotine vaccine differ according to vaccine Formulation and administration conditions. Plos One. 2013; 8
20. de Villiers SHL, Cornish KE, Troska AJ, Pravetoni M, Pentel PR. Increased efficacy of a trivalent nicotine vaccine compared to a dose-matched monovalent vaccine when formulated with alum. Vaccine. 2013; 31:6185–6193. [PubMed: 24176492]
21. Keyler DE, Roiko SA, Earley CA, Murtaugh MP, Pentel PR. Enhanced immunogenicity of a bivalent nicotine vaccine. Int. Immunopharmacol. 2008; 8:1589–1594. [PubMed: 18656557]
22. Pravetoni M, Keyler DE, Pidaparthi RR, Carroll FI, Runyon SP, Murtaugh MP, Earley CA, Pentel PR. Structurally distinct nicotine immunogens elicit antibodies with non-overlapping specificities. Biochem. Pharmacol. 2012; 83:543–550. [PubMed: 22100986]
23. Chen XY, Pravetoni M, Bhayana B, Pentel PR, Wu MX. High immunogenicity of nicotine vaccines obtained by intradermal delivery with safe adjuvants. Vaccine. 2012; 31:159–164. [PubMed: 23123021]
24. Storni T, Kundig TM, Senti G, Johansen P. Immunity in response to particulate antigen-delivery systems. Adv. Drug. Deliver. Rev. 2005; 57:333–355.
25. Benne N, van Duijn J, Kuiper J, Jiskoot W, Slutter B. Orchestrating immune responses: How size, shape and rigidity affect the immunogenicity of particulate vaccines. J. Control. Release. 2016; 234:124–134. [PubMed: 27221070]
26. Pentel PR, LeSage MG. New Directions in Nicotine Vaccine Design and Use. Adv. Pharmacol. 2014; 69:553–580. [PubMed: 24484987]
27. Thangavel S, Yoshitomi T, Sakharkar MK, Nagasaki Y. Redox nanoparticle increases the chemotherapeutic efficiency of pioglitazone and suppresses its toxic side effects. Biomaterials. 2016; 99:109–123. [PubMed: 27235996]
28. Liu J, Wei T, Zhao J, Huang YY, Deng H, Kumar A, Wang CX, Liang ZC, Ma XW, Liang XJ. Multifunctional aptamer-based nanoparticles for targeted drug delivery to circumvent cancer resistance. Biomaterials. 2016; 91:44–56. [PubMed: 26994877]
29. Yeom JH, Lee B, Kim D, Lee JK, Kim S, Bae J, Park Y, Lee K. Gold nanoparticle-DNA aptamer conjugate-assisted delivery of antimicrobial peptide effectively eliminates intracellular Salmonella enterica serovar Typhimurium. Biomaterials. 2016; 104:43–51. [PubMed: 27424215]
30. Rosalia RA, Cruz LJ, van Duikeren S, Tromp AT, Silva AL, Jiskoot W, de Gruijl T, Lowik C, Oostendorp J, van der Burg SH, Ossendorp F. CD40-targeted dendritic cell delivery of PLGA-nanoparticle vaccines induce potent anti-tumor responses. Biomaterials. 2015; 40:88–97. [PubMed: 25465442]
31. Qian Y, Jin HL, Qiao S, Dai YF, Huang C, Lu LS, Luo QM, Zhang ZH. Targeting dendritic cells in lymph node with an antigen peptide-based nanovaccine for cancer immunotherapy. Biomaterials. 2016; 98:171–183. [PubMed: 27192420]
32. Wang C, Li P, Liu LL, Pan H, Li HC, Cai LT, Ma YF. Self-adjuvanted nanovaccine for cancer immunotherapy: Role of lysosomal rupture-induced ROS in MHC class I antigen presentation. Biomaterials. 2016; 79:88–100. [PubMed: 26702587]
33. Rahimian S, Kleinovink JW, Fransen MF, Mezzanotte L, Gold H, Wisse P, Overkleeft H, Amidi M, Jiskoot W, Lowik CW, Ossendorp F, Hennink WE. Near-infrared labeled, ovalbumin loaded polymeric nanoparticles based on a hydrophilic polyester as model vaccine: In vivo tracking and evaluation of antigen-specific CD8+ T cell immune response. Biomaterials. 2015; 37:469–477. [PubMed: 25453974]
34. Hu Y, Ehrich M, Fuhrman K, Zhang CM. In vitro performance of lipid-PLGA hybrid nanoparticles as an antigen delivery system: lipid composition matters. Nanoscale Res. Lett. 2014; 9
35. Zheng H, Hu Y, Huang W, de Villiers S, Pentel P, Zhang JF, Dorn H, Ehrich M, Zhang CM. Negatively charged carbon nanohorn supported cationic liposome nanoparticles: a novel delivery vehicle for anti-nicotine vaccine. J. Biomed. Nanotechnol. 2015; 11:2197–2210. [PubMed: 26510313]
36. Harris JR, Markl J. Keyhole limpet hemocyanin (KLH): a biomedical review. Micron. 1999; 30:597–623. [PubMed: 10544506]

37. McCluskie MJ, Thorn J, Mehelic PR, Kolhe P, Bhattacharya K, Finneman JI, Stead DR, Piatchek MB, Zhang NL, Chikh G, Cartier J, Evans DM, Merson JR, Davis HL. Molecular attributes of conjugate antigen influence function of antibodies induced by anti-nicotine vaccine in mice and non-human primates. Int. Immunopharmacol. 2015; 25:518–527. [PubMed: 25737198]

38. Collins KC, Janda KD. Investigating hapten clustering as a strategy to enhance vaccines against drugs of abuse. Bioconjugate Chem. 2014; 25:593–600.

39. Foged C, Brodin B, Frokjaer S, Sundblad A. Particle size and surface charge affect particle uptake by human dendritic cells in an in vitro model. Int. J. Pharm. 2005; 298:315–322. [PubMed: 15961266]

40. Bachmann MF, Jennings GT. Vaccine delivery: a matter of size, geometry, kinetics and molecular patterns. Nat. Rev. Immunol. 2010; 10:787–796. [PubMed: 20948547]

41. Reddy ST, van der Vlies AJ, Simeoni E, Angeli V, Randolph GJ, O'Neill CP, Lee LK, Swartz MA, Hubbell JA. Exploiting lymphatic transport and complement activation in nanoparticle vaccines. Nat. Biotechnol. 2007; 25:1159–1164. [PubMed: 17873867]

42. Oussoren C, Zuidema J, Crommelin DJ, Storm G. Lymphatic uptake and biodistribution of liposomes after subcutaneous injection. II. Influence of liposomal size, lipid compostion and lipid dose. Biochim. Biophys. Acta. 1997; 1328:261–272. [PubMed: 9315622]

43. Banchereau J, Steinman RM. Dendritic cells and the control of immunity. Nature. 1998; 392:245–252. [PubMed: 9521319]

44. Maurer P, Jennings GT, Willers J, Rohner F, Lindman Y, Roubicek K, Renner WA, Muller P, Bachmann MF. Frontline: A therapeutic vaccine for nicotine dependence: preclinical efficacy, and phase I safety and immunogenicity. Eur. J. Immunol. 2005; 35:2031–2040. [PubMed: 15971275]

45. Liu XW, Xu Y, Yu T, Clifford C, Liu Y, Yan H, Chang Y. A DNA nanostructure platform for directed assembly of synthetic vaccines. Nano Lett. 2012; 12:4254–4259. [PubMed: 22746330]

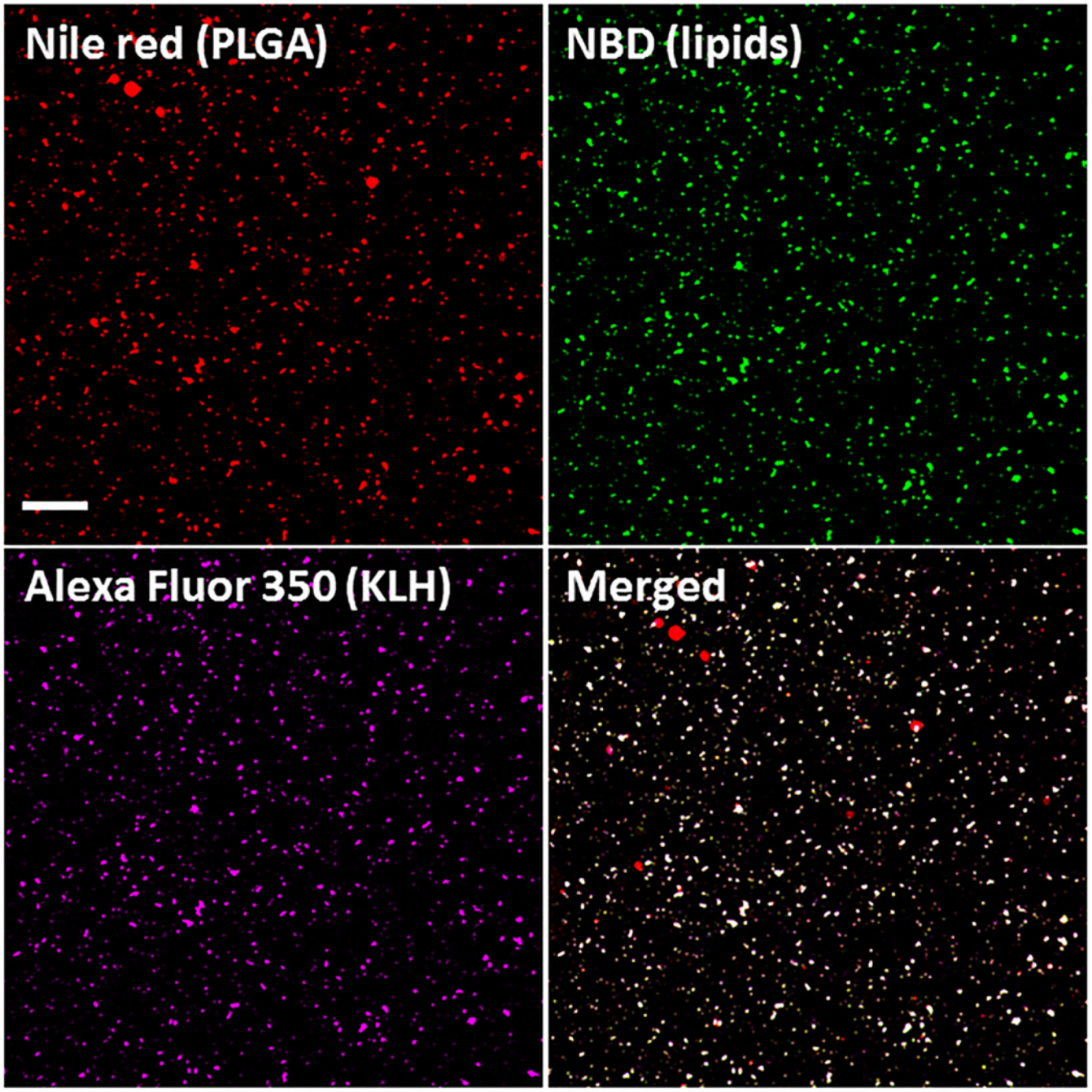

Fig. 1.

Validation of the successful assembly of nanovaccine NPs by CLSM. The PLGA and lipid layer were labeled by Nile red and NBD, respectively, and AF350 was used as a model of Nic hapten attached on KLH. The scale bar represents 10 μm.

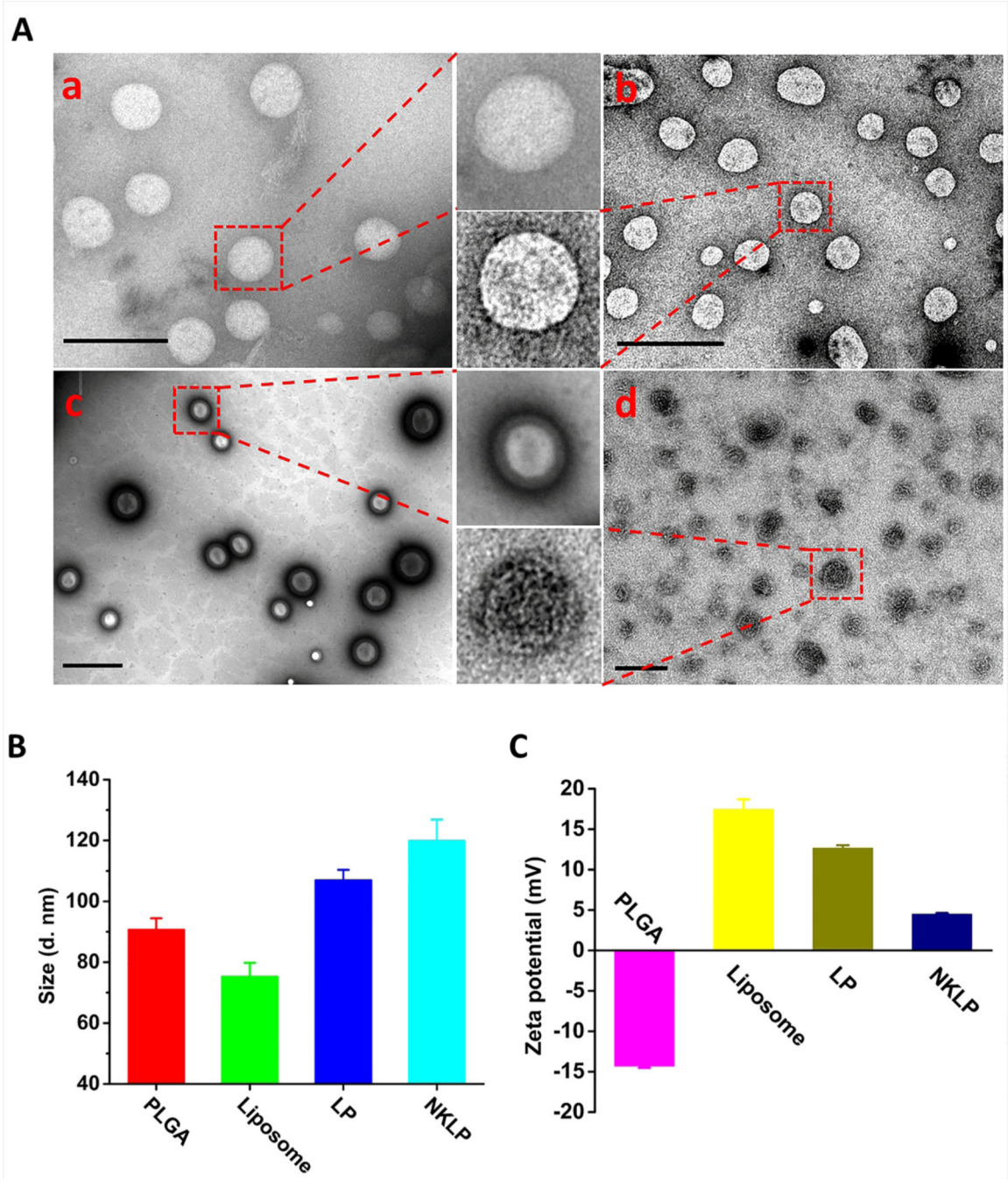

Fig. 2.

Morphological and physicochemical properties of NPs involved in the preparation of nanovaccine NPs. (A) TEM images of (a) PLGA NPs; (b) liposome NPs; (c) lipid-PLGA hybrid NPs; and (d) nanovaccine NPs. Scale bars in all the TEM images represent 200 nm. (B) Average size of NPs. (C) Zeta potential of NPs.

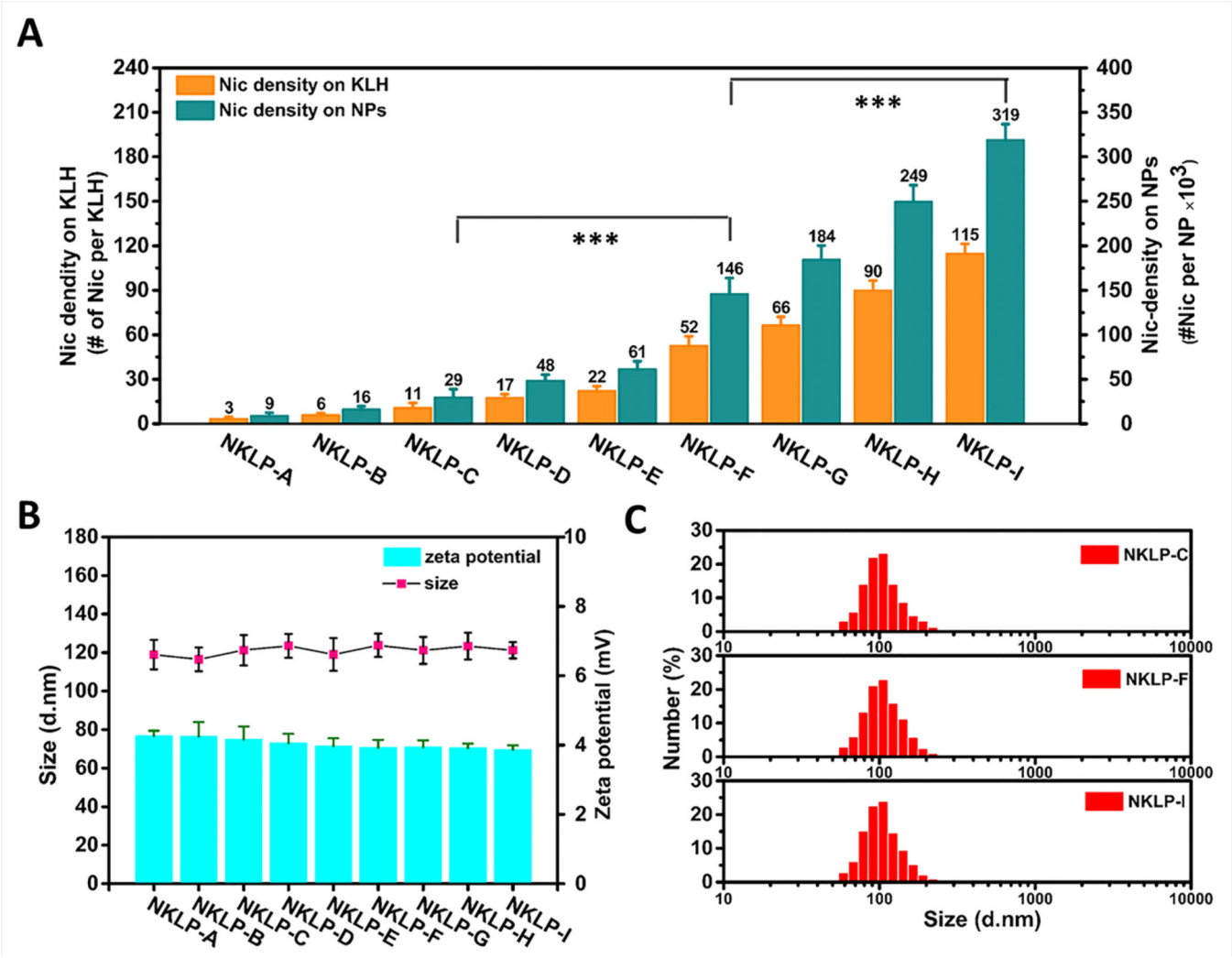

Fig. 3.

Characterization of the hapten density and physicochemical properties of different hapten density nanovaccine NPs. (A) Hapten density of different nanovaccines, which were prepared using various molar ratios of Nic-hapten to KLH. *** indicates hapten density on NPs are significantly different (p-value < 0.001). (B) Average diameter and zeta potential of various NPs. No significant differences in average size detected for all the nanovaccine NPs with different hapten density. (C) Size distribution of three representative nanovaccine NPs used for immunization of mice. NKLP-A, B, C, D, E, F, G, H, I represent nanovaccines which were prepared using increased Nic/KLH molar ratios.

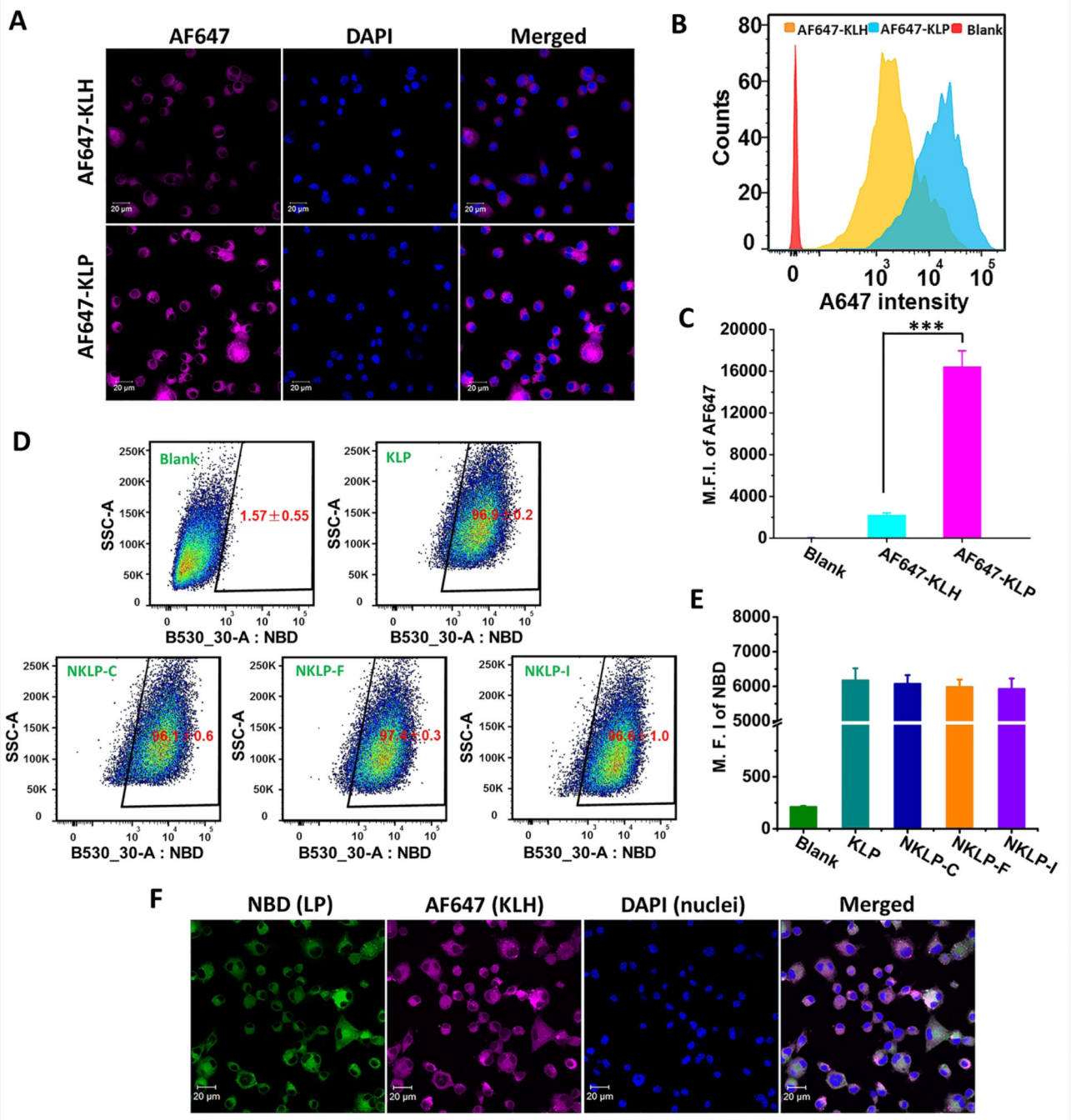

Fig. 4.

Cellular uptake of the lipid-PLGA NP based nanovaccine and conjugate vaccine particles by dendritic cells. (A) CLSM images showing the uptake of nanovaccine and conjugate vaccine particles. (B) Representative intensity distribution of AF647 fluorescence in dendritic cells. (C) Mean fluorescence intensity (M.F.I.) of AF647 in cells corresponding to (B). *** indicates that AF647 fluorescence intensity was significantly higher in AF647-KLP group than in AF647-KLH group ($p<0.001$). For particles used in (A–C), AF647 was conjugated to KLH as a model of Nic-hapten. For (A–C), Cells were treated with nanovaccine or

conjugate vaccine particles containing equal amounts of KLH for 2 h. (D) Recorded events which indicated that most of the studied cells (>95%) had taken up NPs of KLP, NKLP-C, NKLP-F, and NKLP-I, after 2 hours' incubation. The percentages of positive cells were shown in red figures. (E) M.F.I of AF647 in cells after internalizing NPs for 2 h. NPs used in (D) and (E) were labeled by adding NBD to the lipid layer, and cells were treated with equal amounts of different hapten density nanovaccine NPs. (F) CLSM images of cells treated with fluorescent nanovaccine NPs for 2 h, in which the lipid layer was labeled by NBD and AF647 was used as a model of Nic hapten.

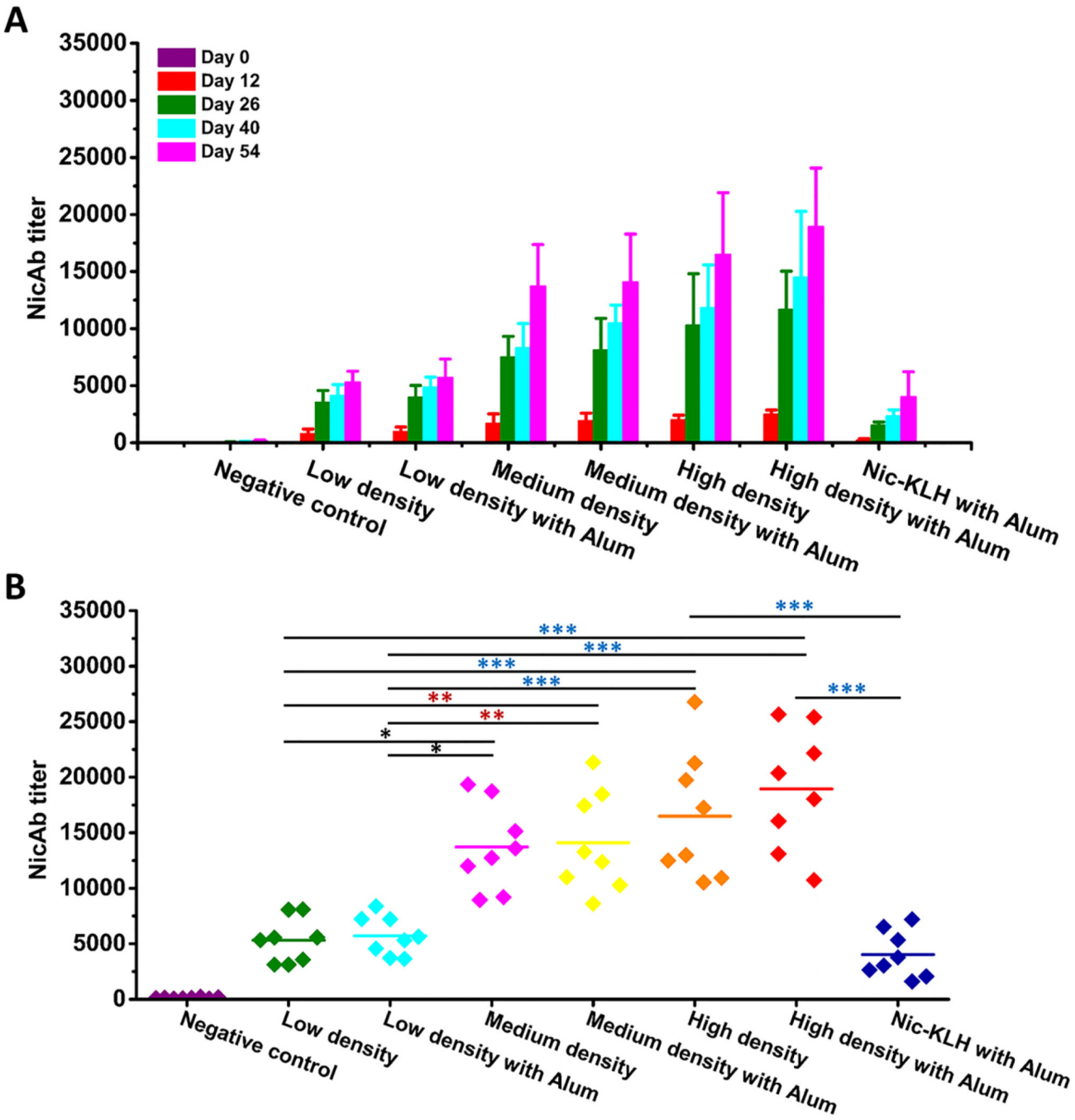

Fig. 5.

Immunogenicity of nicotine vaccines in mice. (A) Time-course of nicotine-specific antibody (NicAb) titers in response to the Nic-KLH conjugate vaccine and hybrid NP-based nanovaccines. (B) Statistical comparison of the NicAb titers on Day 54. Each diamond represents NicAb titer of each mouse, and the colorful straight lines show the average NicAb titer of each group. Significantly different: * $p<0.05$, ** $p<0.01$, *** $p<0.001$.

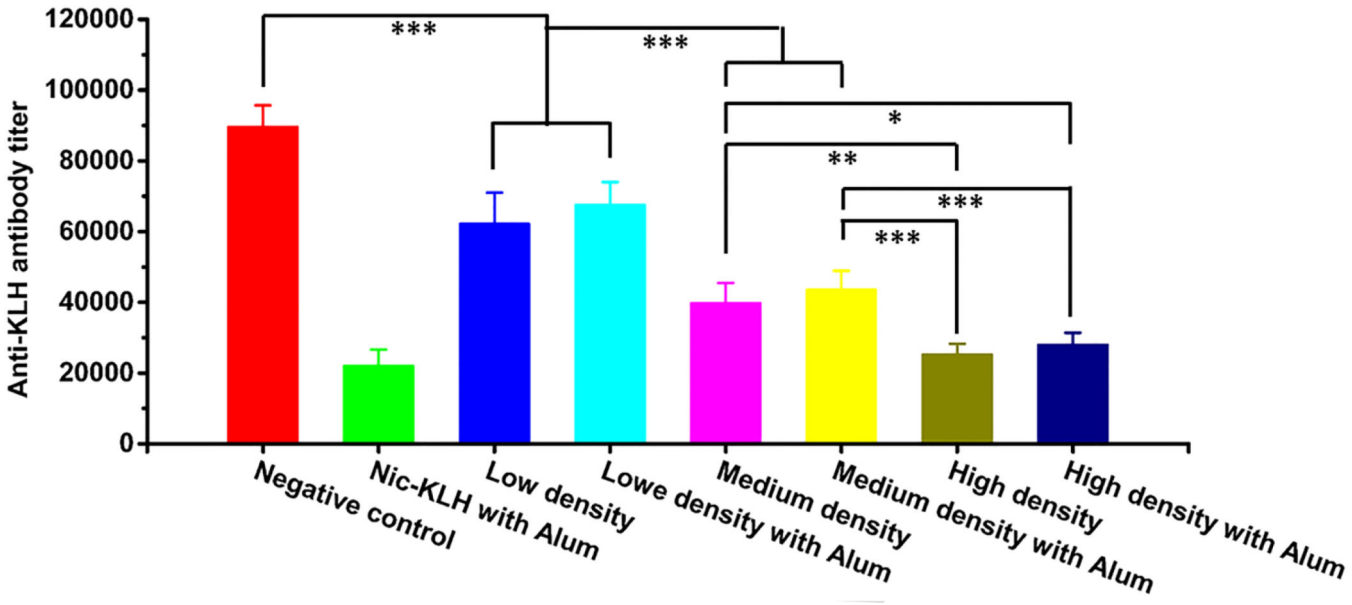

Fig. 6.

Anti-carrier protein (anti-KLH) antibody titers induced by nicotine vaccines on Day 54. Significantly different: * $p<0.05$, ** $p<0.01$, *** $p<0.001$.

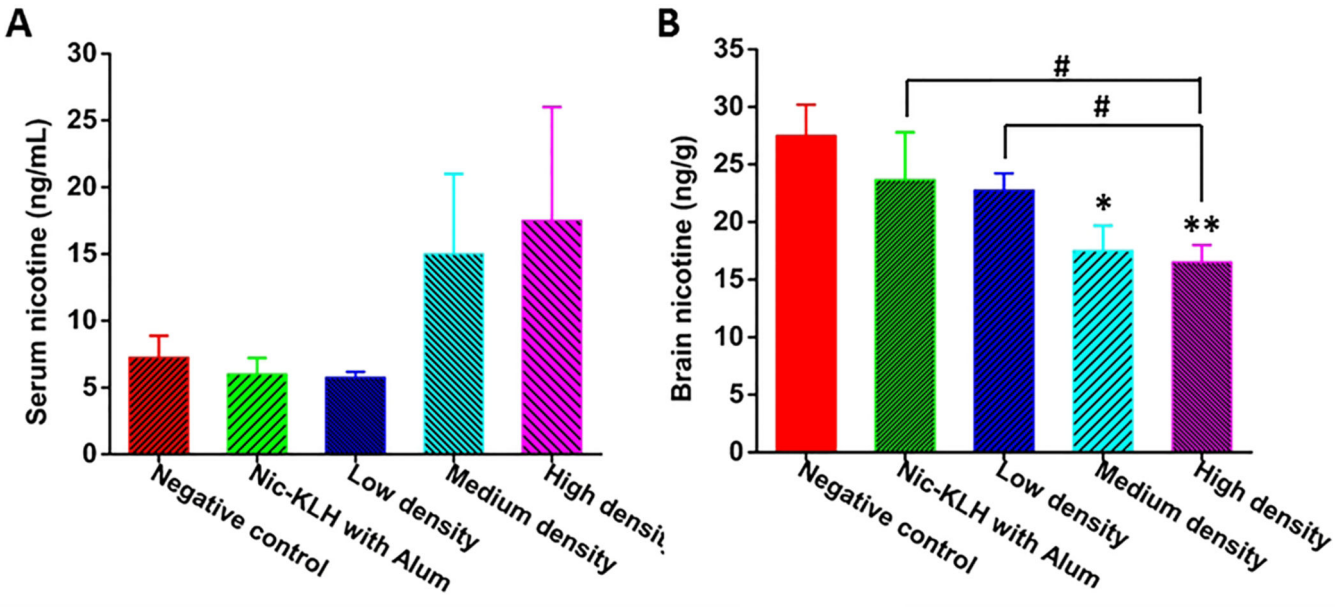

Fig. 7.

Nicotine distribution in the (A) serum and (B) brain of immunized mice. Serum and brain tissues of mice were collected 4 min after administration of 0.03 mg/kg nicotine subcutaneously on Day 54, and nicotine contents in tissues were analyzed. * and ** indicate significant differences compared to the negative control group, * $p<0.05$, ** $P<0.01$; # $P<0.05$.

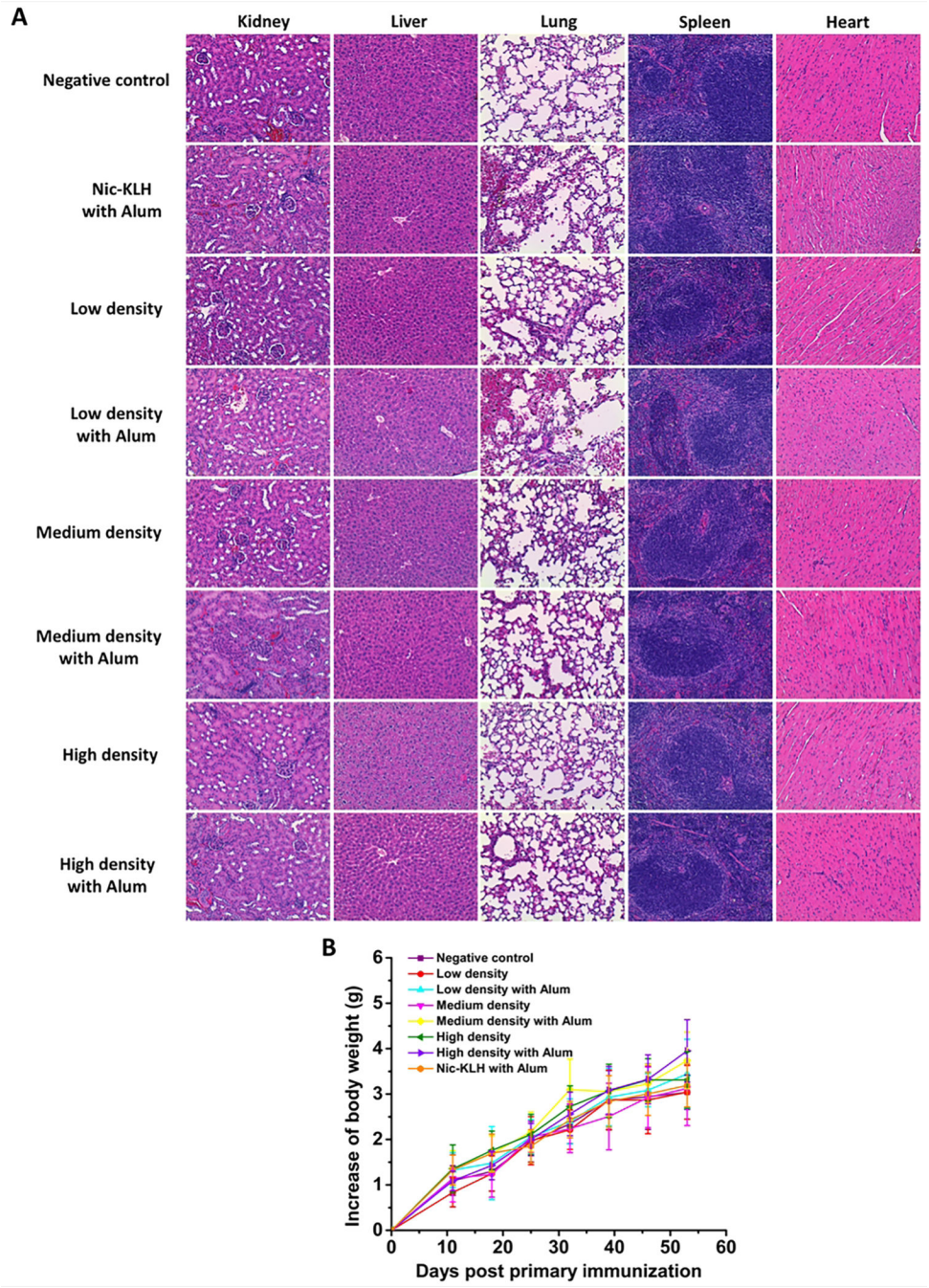

Fig. 8.

Assessment of the safety of nicotine vaccines. (A) Representative histopathological images of mouse tissues after administration of the negative control or nicotine vaccines. No lesions were observed in mouse organs of all the representative groups. (B) The increase of body weight during the immunization study.

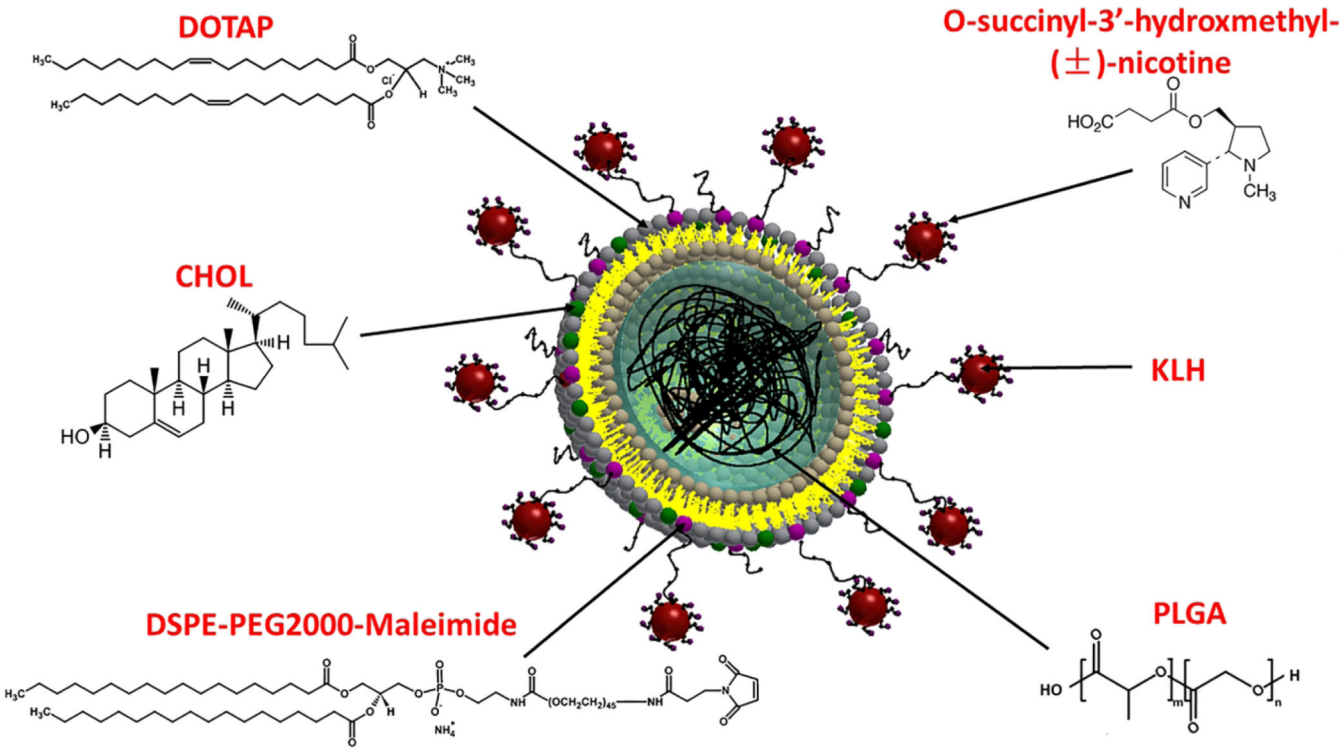

Scheme. 1.
Schematic illustration of the structure of hybrid NP-based nicotine nanovaccine NPs.

Table 1

Physicochemical properties and hapten density of nanovaccine NPs.

NPs	Size (d. nm)	Zeta potential (mv)	PDI	Nic-KLH association efficiency (%)	Hapten density (#×10^3/NP)
NKLP-C (low-density)	121.3±7.9	4.16±0.14	0.22±0.02	86.4±0.97	29.4±9.2
NKLP-F (medium-density)	123.8±6.1	3.92±0.23	0.24±0.03	87.9±1.02	145.6±18.1
NKLP-I (high-density)	121.2±4.2	3.86±0.12	0.21+0.02	86.7±0.45	318.6±18.2